



HAL
open science

New insights into the mechanism of photodegradation of chitosan

Pierre-Olivier Bussiere, Jean-Luc Gardette, Géraldine Rapp, Claire Masson, Sandrine Therias

► To cite this version:

Pierre-Olivier Bussiere, Jean-Luc Gardette, Géraldine Rapp, Claire Masson, Sandrine Therias. New insights into the mechanism of photodegradation of chitosan. Carbohydrate Polymers, Elsevier, 2021, 259, pp.117715. 10.1016/j.carbpol.2021.117715 . hal-03169382

HAL Id: hal-03169382

<https://hal.uca.fr/hal-03169382>

Submitted on 12 Nov 2021

HAL is a multi-disciplinary open access archive for the deposit and dissemination of scientific research documents, whether they are published or not. The documents may come from teaching and research institutions in France or abroad, or from public or private research centers.

L'archive ouverte pluridisciplinaire **HAL**, est destinée au dépôt et à la diffusion de documents scientifiques de niveau recherche, publiés ou non, émanant des établissements d'enseignement et de recherche français ou étrangers, des laboratoires publics ou privés.



Distributed under a Creative Commons Attribution| 4.0 International License

1 **New insights into the mechanism of photodegradation of chitosan**

2 Pierre-Olivier Bussière, Jean-Luc Gardette

3 Géraldine Rapp, Claire Masson and Sandrine Therias*

4 Université Clermont Auvergne, CNRS, SIGMA Clermont, ICCF

5 F-63000 Clermont-Ferrand, France

6
7
8 **Abstract**

9
10 (150 words)

11 Chitosan films were subjected to accelerated artificial weathering at $\lambda > 300$ nm and 60°C in
12 the presence of O₂. The resulting variations in the chemical structure were characterized by IR
13 spectroscopy and UV-visible spectroscopy, and a photooxidation mechanism was proposed
14 based on the identified oxidation photoproducts. The formation of gluconolactone derivatives
15 leading to chain scissions was shown. In addition, low molecular weight photoproducts,
16 which accounted for chitosan deacetylation, were detected. Furthermore, crosslinking
17 reactions occurred, as revealed by gel fraction characterization. Variations in the mechanical
18 and surface properties were characterized by AFM, and the reduction in macroscopic
19 properties was correlated with the structural changes observed at the molecular scale by a
20 multiscale approach.

21
22
23
24
25 **Keywords:** chitosan; photodegradation; oxidation; mechanism

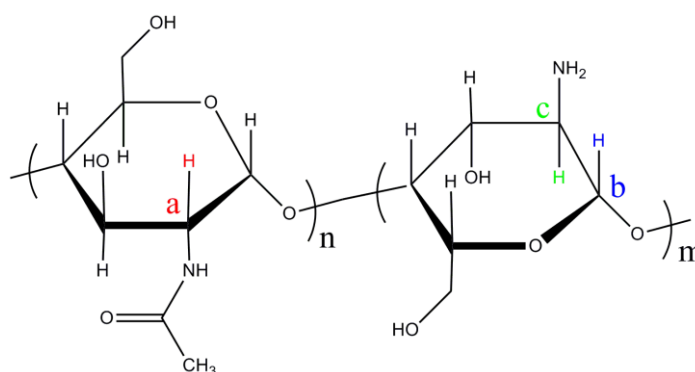
26 *Corresponding author:

27 E-mail addresses: pierre-olivier.bussiere@sigma-clermont.fr (P.O. Bussiere),
28 luc.gardette@uca.fr (J.L. Gardette), geraldine.rapp@uca.fr (G. Rapp), claire.poncet@uca.fr
29 (C. Masson), sandrine.therias@uca.fr (S. Therias)

32 **1. Introduction**

33 Chitosan is a natural polysaccharide composed of N-acetyl glucosamine and glucosamine
34 units, two derivatives of glucose, that are linked together by glycosidic bonds (Synytsya,
35 Grafova, Slepicka, Gedeon & Synytsya, 2012) (Scheme 1). The presence of hydroxyl and
36 amino groups promotes H bonds between macromolecular chains. Thus, chitosan can
37 crystallize into a hydrated form and an anhydrous form (Ogawa, Yui & Okuyama, 2004). Due
38 to its solubility in water, biodegradability, biocompatibility and non-toxicity, many studies
39 have focused on the use of chitosan for medical purposes such as soft tissue engineering
40 (Tchemtchoua et al., 2011), bone tissue engineering (Nazeer, Yilgor, Yilgor, 2017) and drug
41 release (Lien et al., 2012). Due to the same “green” characteristics, chitosan was studied to be
42 employed as a scaffold for water treatment (Moczek & Nowakowska, 2007) and as packaging
43 material in the food industry (Aider, 2010).

44
45
46



47
48
49

Scheme 1: Chemical structure of chitosan

50 The dependence of the thermal degradation of chitosan on the degree of deacetylation was
51 studied (Gamiz-Gonzalez et al., 2017), (Villar-Chavero, Dominguez, Alonso, Oliet &
52 Rodriguez, 2018). Changes in the degree of deacetylation of chitosan were reported during
53 thermal treatment above 200°C (Zawadzki & Kaczmarek, 2010). The effect of the degree of
54 deacetylation on the radiation-induced degradation of chitosan (Taskn, Cansag, Sen, 2014)
55 was also investigated and revealed that deacetylation is an important factor for controlling the
56 degradation rate of chitosan. Degradation of chitosan under different stresses (microwave
57 (Wasikiewicz & Yeates, 2013) and cavitation (Huang, Wu, Huang, Yang & Ren, 2013) has
58 also been reported. Regarding photodegradation, a few papers report the use of UV irradiation
59 as a sterilizing agent at a wavelength of 254 nm: chitosan (Sionkowska, Planecka,

60 Lewandowska, Kaczmarek & Szarszewska, 2013) (Andrady, Torikai, Kobatake, 1996)
61 (Mucha &Pawlak, 2002); blends of chitosan/poly(vinyl pyrrolidone) (Sionkowska,
62 Wisniewski, Skopinska, Vicini & Marsano, 2005) and of chitosan/poly(ethylene oxide)
63 (Kowalonek, 2017); and chitosan modified with keratin (Sionkowska, Skopinska-
64 Wisniewska, Planecka & Kozłowska, 2010), with silk fibroin (Sionkowska, Planecka,
65 Lewandowska & Michalska, 2014) or with tannic acid (Sionkowska, Kaczmarek, Gnatowska
66 & Kowalonek, 2015). The effect of UV degradation was mainly characterized on the thermal
67 or mechanical properties but also on the surface of chitosan films (Sionkowska, 2006). UV
68 irradiation at $\lambda = 254$ nm was shown to provoke a decrease in molecular weight as a result of
69 chain scissions. Changes in IR spectra were observed, such as the formation of bands
70 attributed to carbonyl groups at 1730 cm^{-1} and an increase of bands attributed to amide at
71 1655 cm^{-1} (C=O) and 1560 cm^{-1} (N-H) accompanied with a decrease of the IR band at 1590
72 cm^{-1} corresponding to the amine group (Sionkowska et al; 2013) (Mucha &Pawlak, 2002).
73 One study reports the TiO_2 photocatalytic-oxidation of solid-state chitosan under fluorescent
74 irradiation (Nawi, Jawad, Sabar & Wan Ngah, 2011); more recently, the effect of UV
75 irradiation on the physicochemical characteristics of chitosan modified with nanoparticles of
76 silver vanadate (Abdelghany, Ayaad & Aboelkheir, 2019) was reported. However, weathering
77 of chitosan films under UV-light irradiation at long wavelengths ($\lambda > 300$ nm) under
78 accelerated conditions of natural outdoor weathering has received little attention
79 (Sionkowska, Planecka, Kozłowska, Skopinska-Wisniewska, Los, 2011), and no mechanism
80 of photooxidation has been proposed.

81 The aim of this work is to propose a photodegradation mechanism of chitosan in
82 photooxidative conditions at $\lambda > 300$ nm under accelerated artificial conditions (at 60°C in the
83 presence of O_2), which can explain the variations in material properties. The main objective of
84 the paper is to provide evidence of the consequences of photochemical reactions on the
85 macroscopic properties of chitosan and to qualitatively and quantitatively confirm the direct
86 relationship between variations in the chemical structure and variations in the mechanical
87 properties due to a multiscale approach of the degradation.

88

89 **2. Experimental**

90 **2.1. Materials**

91

92 Chitosan was purchased from Polysciences Inc. as a purified powder with an average
93 molecular weight of 15 000 g.mol⁻¹ and a minimum degree of deacetylation of 85%. –Thus,
94 the R group in Scheme 1 is defined as –H for 85 % of monomer and as acetamide group for
95 15 % of monomer. The deacetylation degree of the chitosan film (after Soxhlet treatment) was
96 monitored using IR spectra by following the formula given by Kasaai (Kasaai, 2008) for the
97 ratio of absorbance at 1655 cm⁻¹ and 3450 cm⁻¹, at 1320 cm⁻¹ and 1420 cm⁻¹, and at 1560 cm⁻¹
98 and 2875 cm⁻¹. The degree of deacetylation was then estimated to be 82 ± 4 %, and the NH₂
99 group predominated the acetamide group in this chitosan sample.

100 To prepare the films, chitosan powder was dissolved in acidified water (acetic acid 1%
101 v/v, pH = 5) at a concentration of 10-20 mg.mL⁻¹ and stirred for 3 h at 60°C. Solutions were
102 then deposited in Petri dishes, and self-standing films were obtained after drying in ambient
103 air for a few hours. Films of thickness in the range 25 – 50 µm or 150 µm were obtained for
104 the different subsequent analyses. Purification of the films was performed by Soxhlet
105 extraction in MeOH for 24 h. The films were then dried at 60°C under vacuum for 14 hours.

106

107 **2.2. Irradiation**

108 UV-visible light irradiation ($\lambda > 300$ nm) of thin films was performed in a SEPAP
109 12/24 unit, which was designed for studying polymer photodegradation during artificial
110 ageing with medium-accelerated conditions (Philippart, Sinturel & Gardette, 1997). The
111 chamber consisted of a square reactor equipped with four medium-pressure mercury lamps
112 situated vertically at each corner of the chamber. Wavelengths below 300 nm were filtered by
113 the borosilicate envelope of the lamps, acting as a UV filter below 300 nm (see Fig S1). In the
114 centre of the chamber, the samples were fixed on a 13 cm-diameter rotating carousel that can
115 hold 24 samples. The temperature in the chamber of SEPAP 12/24 is controlled at the surface
116 of a polymer film through a Pt 1000 probe and continually regulated by air circulation. The
117 temperature at the surface of the samples was set to 60°C.

118

119 **2.3. Characterization Techniques**

120 *Spectroscopic analysis*

121 Changes in the UV-visible spectra were monitored with a Shimadzu 2600 plus
122 spectrophotometer equipped with an integrating sphere. IR spectra were recorded in
123 transmission mode with a Nicolet 6700 Fourier transform infrared (FTIR) spectrophotometer
124 operated with OMNIC software. The spectra were obtained with 32 scan summations at 4 cm⁻¹

125 ¹ resolution. IR analysis of chitosan powder was performed by mixing 2 mg of this powder
126 with 200 mg of KBr.

127

128 *Chemical derivatization reaction*

129 Most of the oxidation products were identified by performing chemical derivatization
130 treatments that selectively convert oxidation products into chemical groups with different IR
131 characteristics (Wilhelm & Gardette, 1994). Ammonia (NH₃) reacts with carboxylic acids to
132 generate carboxylate ions and with esters to generate amides. NH₃ treatment was performed at
133 room temperature in simple flow reactors that could be sealed off to allow the reaction to
134 proceed. 2,4-Dinitrophenylhydrazine (2,4 DNPH) was used to identify aldehydes and ketones.
135 The formation of 2,4-dinitrophenylhydrazone can be detected by two IR absorption bands at
136 1595 cm⁻¹ and 1620 cm⁻¹ and a very intense UV-Vis absorption band at 365 nm.

137

138 *Solid Phase Micro Extraction (SPME)*

139 Films were irradiated in sealed vials to collect the volatile photodegradation products.
140 SPME analysis was performed using Carboxen–PDMS fibres (75 mm) from Supelco
141 (Bellefonte, PA, USA) with an extraction time of 5 min at 60°C, and gas chromatography-
142 mass spectrometry (GC-MS) was performed with a PEG Supelcowax® 10 column (30 m x
143 0.25 mm x 0.25 mm) from Supelco.

144

145 *Gel fraction*

146 Crosslinking of polymers was evaluated by gravimetric measurements of the gel fraction (Gf).
147 Irradiated films (approximately 5 mg) were immersed in acidified water (acetic acid 1% v/v)
148 (5 mL) for 48 h. The solutions were then filtered using a Büchner funnel. The insoluble
149 fractions were dried at 60°C and then weighed. The gel fraction is defined by equation 1:

$$Gf = \frac{M_{\text{insoluble}}}{M_{\text{initial}}} \quad (1)$$

150

151 *Atomic force microscopy*

152 AFM measurements were performed in tapping mode using an atomic force microscope
153 (AFM) Bruker Multimode driven by a Nanoscope V control unit. The surface topographical
154 images were analysed by the Nanoscope 7.20 software. Images were obtained at three
155 different locations, and the average roughness was determined from these images at four

156 different locations for each image. The tip was an RTESPA-300 cantilever (Bruker) with a
157 spring constant of approximately 40 N/m and a radius of curvature of approximately 8 nm.

158

159

160 *AFM nano-indentation*

161 The force–distance curves were measured at a constant deflection (or constant load). Nano-
162 indentations were performed using a diamond tip (64.05 kHz) with a spring constant of 234.5
163 N/m and a curvature radius of 25 nm. Three tests of nano-indentation were performed on
164 different areas of the polymer film. Each test corresponded to nine indentations; thus, 3×9
165 force curves were used with a load that varied from 1 to 5 μN. The force-displacement curves
166 obtained via AFM nano-indentation measurements were analysed using the model proposed
167 by Oliver and Pharr (Oliver & Pharr, 1992) (procedure (O&P)).

168

169 *AFM nanoscale thermal analysis*

170 Variations in the thermal properties of the films were monitored at the surface using an
171 AFM nanoscale thermal analysis module (Vita). The probe was heated from 20°C to 300°C at
172 a rate of 5 °C/s, and each measurement was performed 3 times to ensure good reproducibility.
173 The Vita probes can also be used to obtain AFM images of the surface (Collin et al., 2012).

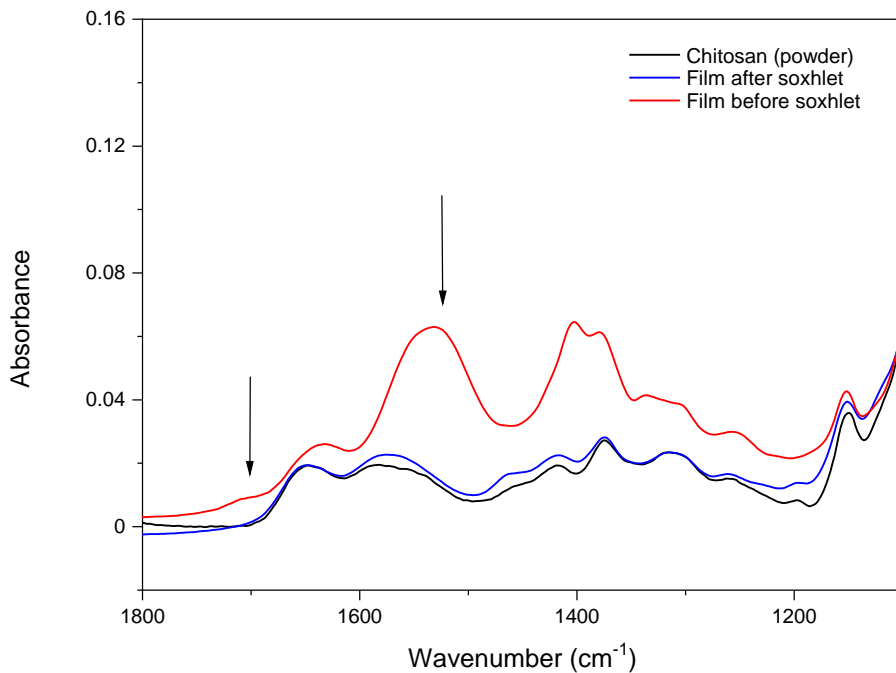
174

175 **3. Results and discussion**

176 **3.1. Characterization of chitosan films before irradiation**

177 The main spectral features of chitosan and assignment of the IR bands according to the
178 literature (Mucha & Pawlak (2002)(Valentin, Bonelli, Garrone, Di Renz &, Quignard, 2007)
179 are the OH and NH stretching bands at 3435 cm⁻¹ and between 3300-3150 cm⁻¹, respectively,
180 the C=O stretching band at 1655 cm⁻¹, the NH₂ scissoring and NH deformation bands at 1590
181 cm⁻¹ and 1560 cm⁻¹ and the C-O-C stretching band attributed to the osidic bond or pyranose
182 ring at 1150 cm⁻¹. Figure 1 compares the carbonyl domain in the IR spectrum of the
183 commercial chitosan powder pressed into a KBr pellet to the same domain in the IR spectra of
184 the pristine films before and after Soxhlet extraction in MeOH for 24 h.

185



186
 187 Figure 1: IR spectra of chitosan films ($e = 25 \mu\text{m}$) before and after 24 h Soxhlet extraction in
 188 MeOH and the chitosan powder in KBr pellets.

189
 190 The IR spectra shown in Figure 1 indicate that Soxhlet extraction of the chitosan film
 191 in MeOH provokes the disappearance of three IR bands at 1710 cm^{-1} , 1550 cm^{-1} and 1410 cm^{-1} .
 192 This finding can be attributed to the removal of acetic acid and acetate ions. These two
 193 products are retained from the process that was used to obtain the films and involved
 194 preliminary dissolution in acetic acid-containing solution, which could therefore be trapped
 195 within the films at low concentrations even after drying. Acetate ammonium groups are likely
 196 generated as a result from the reaction of acetic acid with the amine functions of chitosan
 197 (Rinaudo, Pavlov & Desbrieres, 1999). The IR spectrum of chitosan film after Soxhlet
 198 extraction is similar to the spectrum of chitosan powder that was pressed into KBr pellets. The
 199 experiments reported in this paper were performed for chitosan films that were purified by
 200 Soxhlet extraction in MeOH for 24 h.

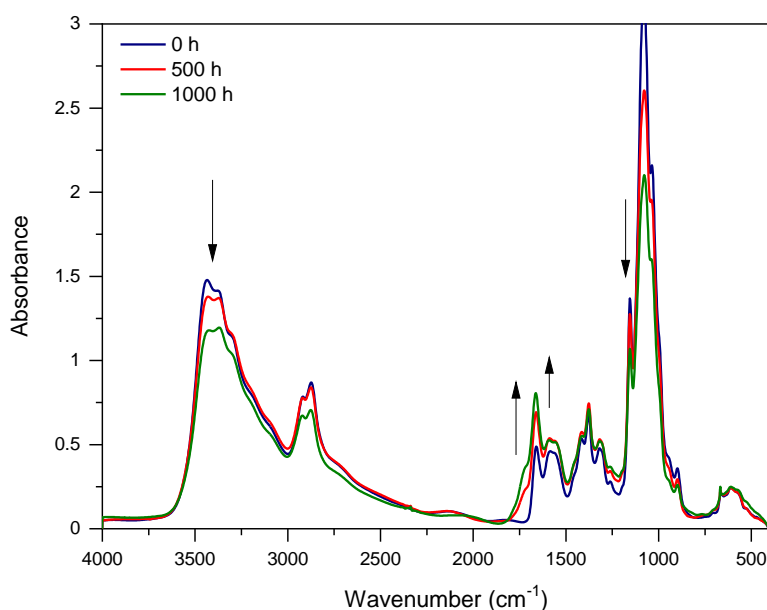
201
 202 **3.2. Photooxidation of chitosan**
 203 **3.2.1. Analysis of chemical variations by IR spectroscopy**

204 Irradiation in accelerated artificial conditions at $\lambda > 300 \text{ nm}$ in the presence of O_2
 205 (photooxidation) resulted in noticeable modifications to the IR spectra (Figure 2a). Irradiation
 206 provoked a marked decrease in the absorption in the domain $3500 - 3300 \text{ cm}^{-1}$, which

207 indicates a loss of constitutive water or water generated from the dissolution process and/or
208 breaking of hydrogen bonds present in the chitosan film (Ogawa et al., 2004). A decrease in
209 the IR absorption band of C-O-C bonds at 1150 cm^{-1} was also observed, which could reflect
210 chain scission reactions and/or ring opening of glucosamine and N-acetyl glucosamine. To
211 visualize the changes in the IR spectra in the carbonyl domain, the spectra were subtracted
212 from those of the unexposed film in the domain $2000\text{-}1500\text{ cm}^{-1}$ and are presented in Figure
213 2b. A relatively broad band was observed, with a maximum at 1675 cm^{-1} and shoulders at
214 1730 cm^{-1} and 1780 cm^{-1} . This result is similar to the 254 nm irradiation-induced spectral
215 variations reported in the literature, which proposed chain scission reactions and cleavage of
216 glycosidic bonds (Andrady et al. 1996) (Mucha & Pawlak, 2002) (Wasikiewicz, Yoshii,
217 Nagasawa, Wach & Mitomo, 2005) (Wang, Huang & Wang, 2005).

218 a)

219



220

221

222

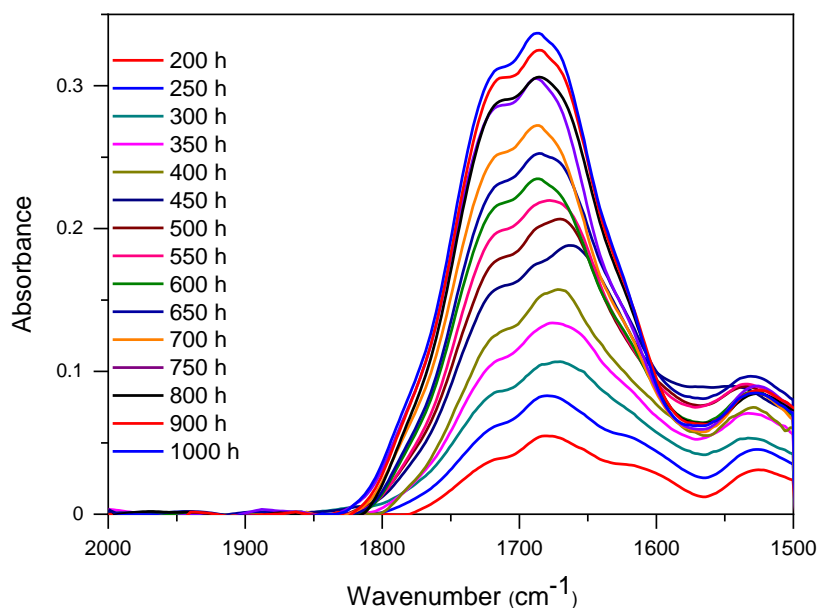
223

224

225

226

227



229

230 Figure 2: a) IR spectra of a chitosan film ($e = 25 \mu\text{m}$) during photooxidation

231 b) Subtracted IR spectra in the carbonyl domain

232

233 The decrease in absorbance at 1150 cm^{-1} (Figure 2) reflects the disappearance of the
 234 pyranose ring/acetal bond and can be correlated with the accumulation of oxidation products
 235 at 1730 cm^{-1} . As proposed by several authors (Mucha & Pawlak, 2002) (Sionkowska, 2011),
 236 the accumulation of oxidation products at 1730 cm^{-1} could be related to the formation of an
 237 ester function and simultaneous disappearance of the β -1,4 osidic bond. Taking into account
 238 the correlation between the increase in absorbance at 1730 cm^{-1} and the decrease at 1150 cm^{-1} ,
 239 which reflects the disappearance of the pyranose ring/acetal bond (hydrogen abstraction on
 240 carbon atom (b) in Scheme 2), this ester bond formation would be consistent with the
 241 generation of gluconolactone.

242 The IR band at 1675 cm^{-1} can be attributed to the vibration $\nu\text{C}=\text{O}$ of a carbonyl function
 243 of amide I. Considering the chemical structure of chitosan, the formation of a primary amide
 244 can also be explained by a mechanism involving oxidation in the α - position of the amine
 245 function (hydrogen abstraction on carbon atom (c)). This mechanism is represented in
 246 Scheme 2 and discussed at a later point in the manuscript.

247

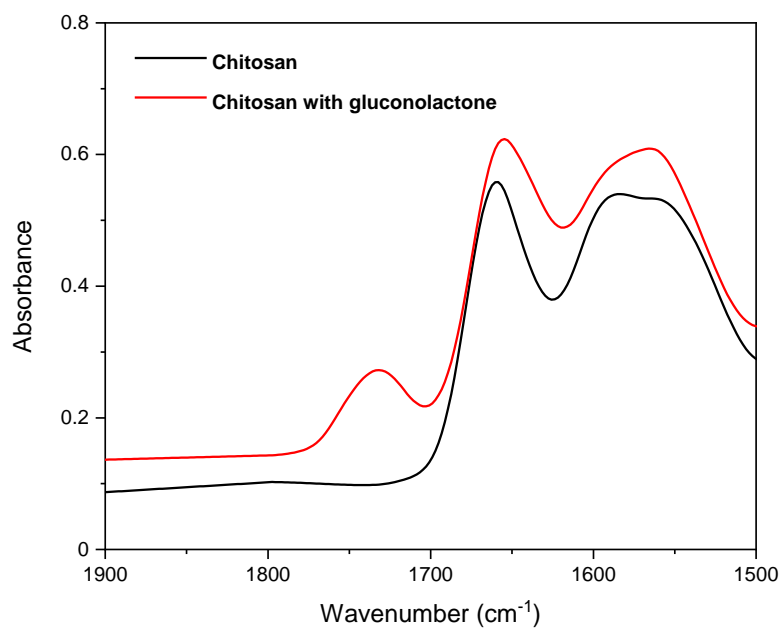
248

249 **3.2.2. Derivatization treatment**

250 Chemical derivatization treatments with NH_3 were performed to identify the
251 degradation products observed by IR analysis at 1730 cm^{-1} . NH_3 reacts with carboxylic acids
252 to generate carboxylate ions and reacts with esters, lactones and anhydrides to generate
253 amides. First, it was verified that no reaction with NH_3 occurred with pristine chitosan. NH_3
254 treatment of photooxidized films provoked a decrease in the broad absorption at 1730 cm^{-1}
255 and the formation of two weak bands at 1640 cm^{-1} and 1595 cm^{-1} (see Fig. S2). These bands
256 indicate the formation of amides (1640 cm^{-1}) and ammonium carboxylates (1595 cm^{-1}).
257 Amides were formed from the reaction of NH_3 with esters or anhydride, and ammonium
258 carboxylates resulted from the reaction of NH_3 with carboxylic acid or anhydrides. NH_3
259 treatment allows the identification of esters and carboxylic acids as oxidation photoproducts.

260 Ester formation was suggested by several authors (Sionkowska et al., 2013), (Andrady
261 et al., 1996) (Mucha & Pawlak, 2002) (Wasikiewicz et al., 2005), but to the best of our
262 knowledge, direct evidence of gluconolactone formation has not yet been reported. For
263 comparison and to confirm the presence of gluconolactone in the photooxidized chitosan film,
264 molecular gluconolactone was blended with pristine chitosan, and the blend was analysed by
265 IR spectroscopy. The IR spectrum is shown in Figure 3a, which clearly confirms the existence
266 of the absorption band at 1730 cm^{-1} attributed to the $\nu(\text{C}=\text{O})$ vibration band of
267 gluconolactone.

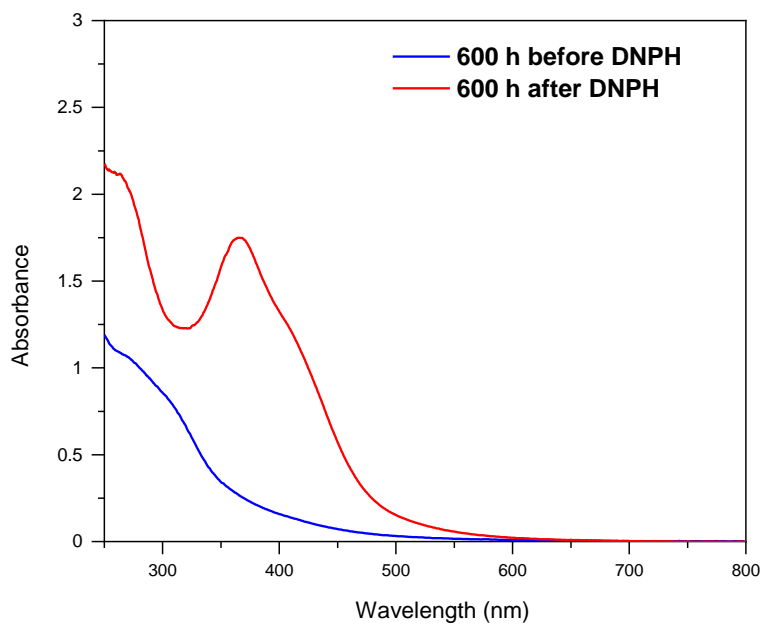
268 a)



269

270 Figure 3a: IR spectrum of a film ($e=25\ \mu\text{m}$) of chitosan blended with gluconolactone.

271 b)



272

273 Figure 3b: UV-visible spectra of a 600 h photooxidized chitosan film before and after
274 treatment with 2,4-DNPH.

275

276 To complete the identification of the oxidation photoproducts, chemical treatment
277 using 2,4-DNPH was performed on photooxidized chitosan films. The UV-visible spectra of
278 photooxidized chitosan films after 2,4-DNPH treatment (Figure 3b) show a broad band with a
279 maximum at 365 nm corresponding to the phenylhydrazone derivative. This result indicates
280 that aldehydes and/or ketones were formed by the photooxidation of chitosan.

281

282

283 ***3.2.3. Analysis of volatile products***

284 Photooxidation of polymers is known to be responsible for the formation of low molecular
285 weight products that are likely to migrate from the solid polymer samples and are not detected
286 by the analysis of the films by the spectroscopic methods reported above (Gaume, Wong-
287 Wah-Chung, Rivaton, Therias, Gardette, 2011). To identify the volatile degradation products,
288 SPME-GC/MS was performed. Formamide and acetamide were detected as the main
289 degradation products (see Figure S3). It is also important to note the presence of acetic acid,
290 which was used to solubilize chitosan. As formamide and acetamide molecules contain
291 nitrogen atoms in their structure and therefore are not formed by photooxidation of the
292 cellulose backbone, these products can be attributed to the degradation of the pending groups
293 of chitosan. As a consequence, the deacetylation degree of the chitosan film is changed.

294 The formation of volatile products (such as acetamide) and the accumulation of
295 ketone/aldehyde groups can be connected to the cleavage of pending groups on carbon atoms
296 (a), following the mechanism given in Scheme 2.

297

298 ***3.2.4. Characterization of chain scission/crosslinking***

299 *Gel fraction*

300 To provide evidence of the variations in polymer architecture, the insoluble/gel
301 fractions of photooxidized chitosan films were measured for irradiation times as long as 400
302 hours. The gel fraction of photooxidized chitosan films increased progressively from 0 (no
303 insoluble fraction before irradiation) to 96 % after 400 hours of irradiation, which indicates
304 that the polymer becomes almost insoluble. This high gel fraction value can be attributed to
305 the formation of a three-dimensional network from crosslinking during the irradiation of
306 chitosan.

307

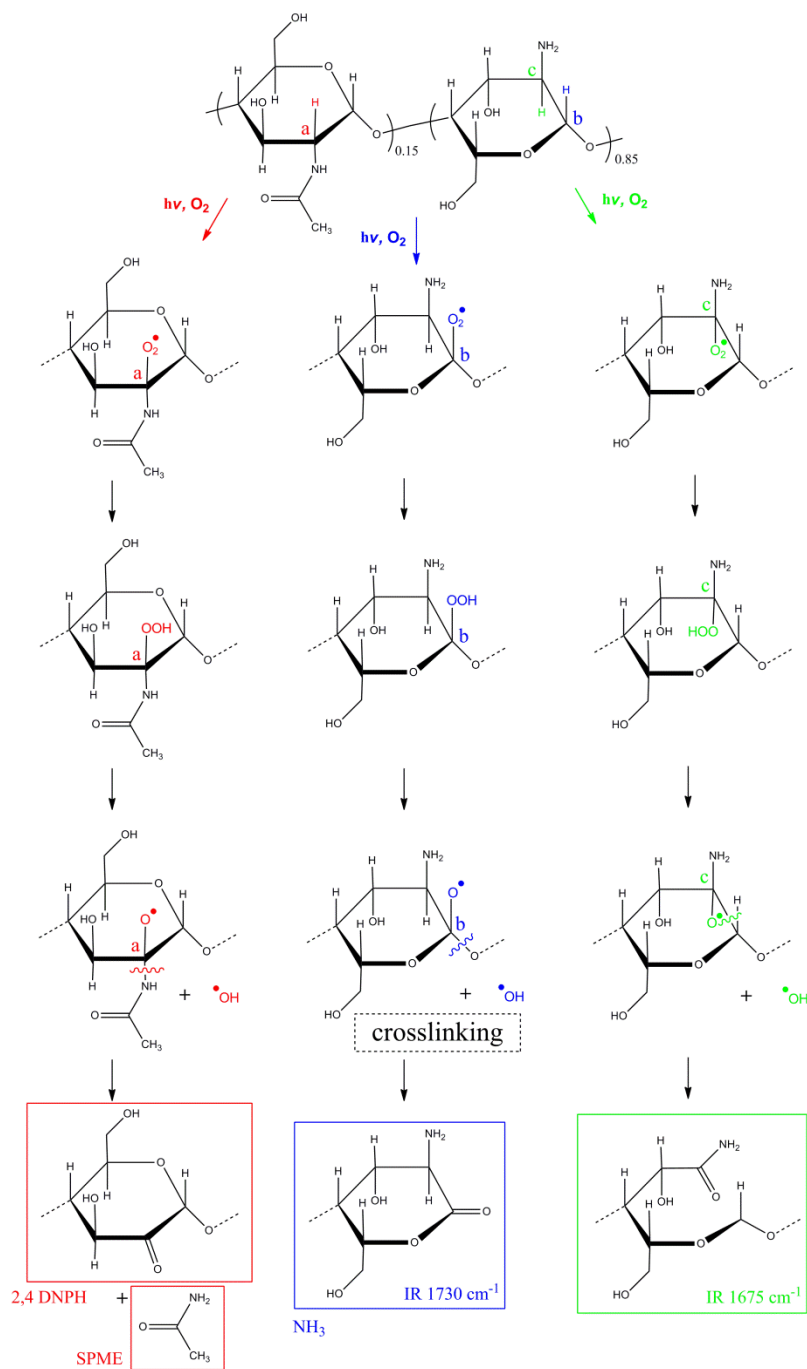
308 **3.3 Degradation mechanism**

309 A photooxidation mechanism that explains the formation of the identified
310 photoproducts was proposed (Scheme 2). This mechanism is based on a radical chain reaction
311 with initial hydrogen abstraction on the carbon atoms noted (a), (b) and (c) by radicals from
312 chromophoric impurities, or defects that in commercial chitosan could include proteins and
313 metals. The photodissociation of acetamide groups attached to glucosamine unit, (broad band
314 from 250 till 350 nm) could also be a potential source of radicals able to initiate the chain
315 reaction. However, despite the many articles published in the literature, no real proof was
316 brought that this reaction occurs on exposure to wavelengths above 300 nm. (Rideal &
317 Mitchell, 1937). However, no evidence was obtained that this reaction would occur (Sharkey
318 & Mochel, 1959). (Moore, 1963). Radical Oxygenated Species such as $\text{HOO}\cdot$, $\text{HO}\cdot$, $\text{R-OO}\cdot$
319 can be formed and initiate the oxidation by hydrogen abstraction on the polymer chains. The
320 initiation processes in polymer degradation have been reviewed many times in the literature
321 (see for example Scott, 1995). This is followed by the addition of dioxygen, the formation of
322 hydroperoxides and the decomposition of hydroperoxides to generate macroalkoxy radicals
323 (Scheme 2). Hydrogen abstraction from the carbon atom (a) generates the macroalkoxy
324 radical A, which may decompose to generate gluconolactone (its IR band at 1730 cm^{-1} was
325 identified by NH_3 treatment). This reaction generates lactones such as gluconolactone and is
326 accompanied by chain scissions. Hydrogen abstraction from carbon (c) leads to the formation
327 of radical C, which may decompose to form amide groups via ring-opening (IR band at 1675
328 cm^{-1}).

329 An important issue is the role played by the temperature in the photooxidation performed at
330 60°C . Thermal ageing at 60°C in a ventilated oven in absence of light (dark control) during
331 the same time (up to 420 h) was then performed. Comparing the IR spectra after exposure for
332 420 h to thermooxidation at 60°C or 400 h to photooxidation at $\lambda > 300\text{ nm}$ - 60°C (see Fig.
333 S4) clearly indicates that the IR spectra was only slightly modified after thermooxidation for
334 420 h, whereas exposure to light at $\lambda > 300\text{ nm}$ - 60°C resulted in dramatic modification of the
335 infrared spectra with the formation of the photoproducts which formation has been described
336 above (part 3.2.1). This result clearly indicates that in the current ageing conditions, the
337 oxidation mainly results from irradiation.

338

339



340

341

342

Scheme 2: Simplified photooxidation mechanism of chitosan

343

344

345 3.4 Consequences of photooxidation on the properties of chitosan

346 3.4.1 UV-visible analysis

347 Analysis of a chitosan film by UV-visible spectroscopy was carried out during
 348 photooxidation (Figure 4).

349

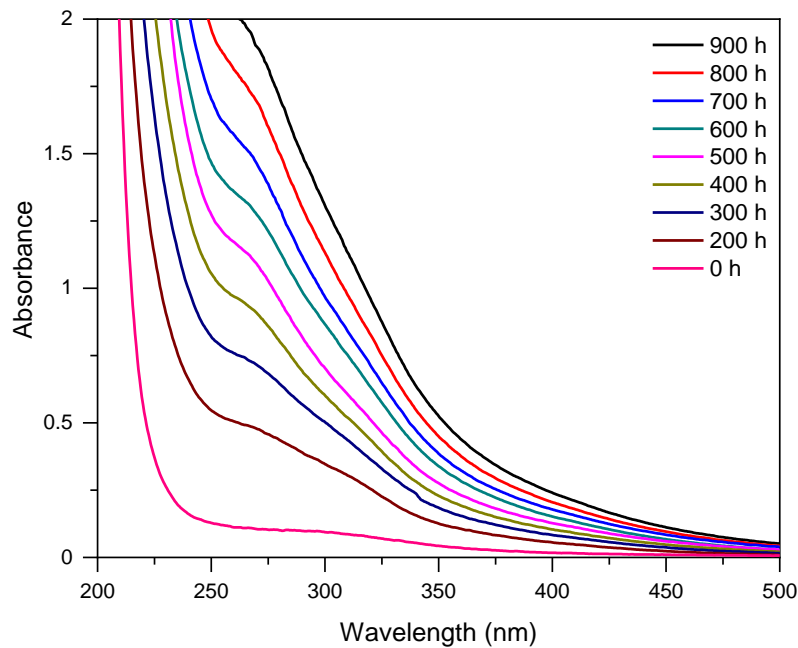


Figure 4: UV-Visible spectra of chitosan films during photooxidation ($e = 25 \mu\text{m}$)

The absorption front of the UV-vis spectra progressively shifted towards longer wavelengths during photooxidation, leading to yellowing of the chitosan film, and a shoulder with an absorption maximum could be observed at 270 nm. This feature was attributed to the formation of carbonyl groups and the cleavage of glycosidic bonds by several authors (Synytsya et al., 2012) (Wang et al., 2005).

3.4.2 Mechanical properties

Variations in the mechanical properties at the surface of chitosan films during photooxidation were assessed by elasticity measurements at the nanoscale (Table 1). To confirm the behaviour at the nanoscale, the polymer surface was analysed by AFM nano-indentation measurements. The loading/unloading indentation curves were measured for two irradiation times (see Figure S5).

The distance or displacement to reach the maximum force decreased after 200 h of irradiation. This is characteristic of an increase in the surface nano-hardness and Young's modulus. The increase in the nano-hardness of chitosan observed under irradiation can be correlated to crosslinking reactions.

371 One can also notice a small negative deflection after 200 h of irradiation that is
372 consistent with the increase in the adhesion work. The increase in the adhesion work with the
373 exposure time has already been connected (Bussiere, Rivaton, Therias & Gardette, 2012) to
374 the accumulation of polar species at the surface of the sample and thus to the formation of
375 oxidation products. In addition, the nano-hardness of the polymer sample can be calculated
376 from these loading-unloading curves.

377

378 *AFM nanoscale thermal analysis*

379

380 In addition, variation in the glass transition temperature resulting from UV light
381 exposure were monitored by AFM thermal analysis (Vita). The deflection-temperature curves
382 (Figure S6) after 100 h and 300 h of irradiation were compared with the deflection-
383 temperature curve before exposure. Nano- T_g values are reported in Table 1. After irradiation,
384 the deflection shifts to higher temperatures. As T_g is related to the deflection, this result
385 indicates that T_g increased with irradiation time. The Flory theory (Fox & Flory, 1950) relates
386 T_g to the molecular weight, reflecting crosslinking reactions.

387

388 Table 1: Evolution of nano-hardness (nano-Hv) and nano- T_g as a function of
389 irradiation time.

Irradiation time	Nano-Hv (at 160 nm)	Nano- T_g (K)
0 h	90 ± 8 MPa	430 ± 5
100 h	150 ± 15 MPa	465 ± 5
200 h	230 ± 25 MPa	495 ± 10
300 h	280 ± 25 MPa	510 ± 5
400 h	330 ± 45 MPa	530 ± 15

390

391 The increase in nano-hardness and nano- T_g are consistent with crosslinking reactions
392 leading to higher molecular weights, with a marked increase in the gel fraction (chitosan that
393 became almost insoluble after 400 h of irradiation at $\lambda > 300$ nm in the presence of oxygen).

394

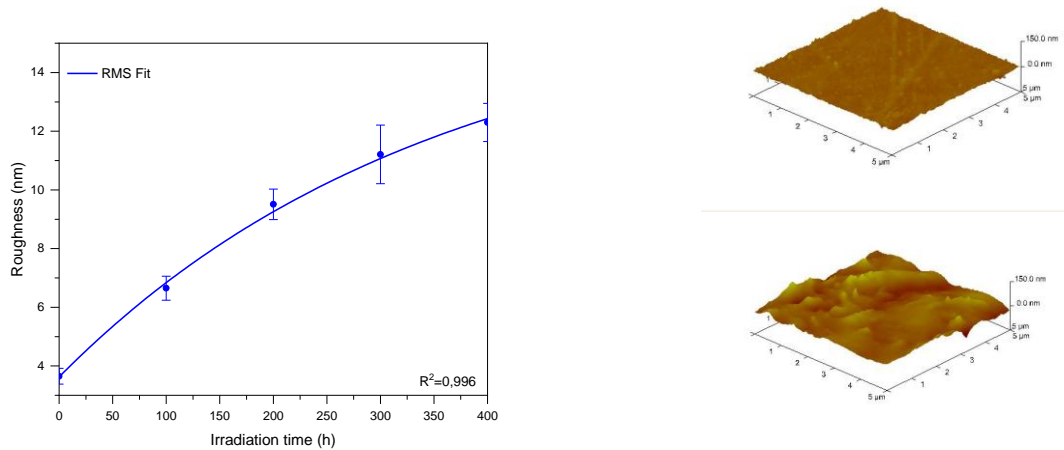
395

396 *3.4.3 Surface properties*

397 Roughness values (RMS) of a chitosan film surface were calculated before and after
398 irradiation. Modifications of the roughness (RMS) displayed in Figure 5 show that RMS
399 increased during irradiation.

400

401



402 Figure 5: a) Change in roughness (■) versus irradiation time

403 (line is obtained by an exponential fit).

404 b) Image of the chitosan film surface before and after 300 hours of irradiation.

405

406 As previously reported, these variations arise from the formation of oxidation products
407 of the polymer sample and of volatile products (Berthumeyrie, Collin, Bussiere & Therias,
408 2014).

409

410

411 3.5 Multiscale correlation

412

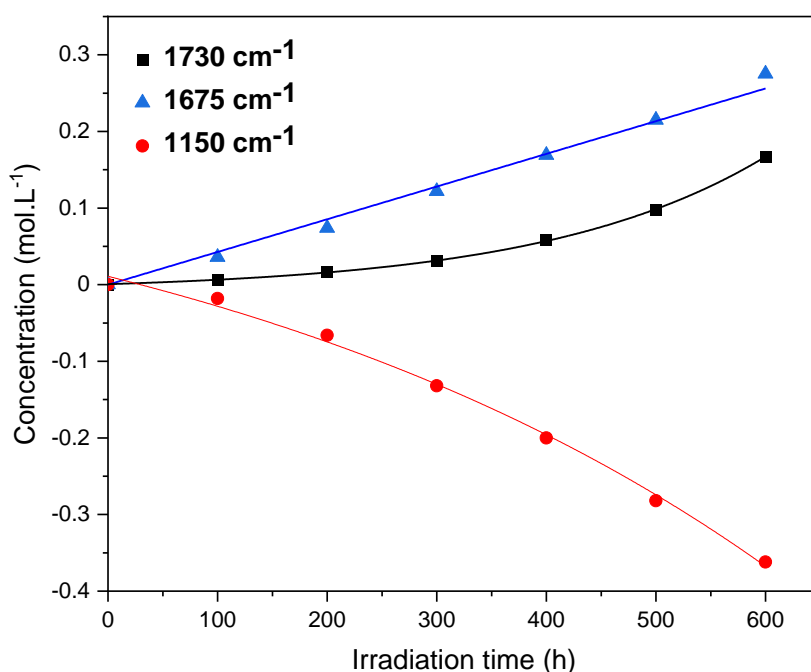
413 As shown above, the degradation of chitosan provoked by exposure to UV light in the
414 presence of air led to variations in the following:

- 415 • chemical structure (oxidation, chain scission/crosslinking)
- 416 • macromolecular architecture (increase in network density, i.e., T_g)
- 417 • mechanical properties (increase in hardness)
- 418 • surface properties (increase in roughness and yellowing).

419

420 Therefore, the degradation caused by exposure to UV light can be characterized by the
421 following parameters: amide and gluconolactone formation, C-O-C conversion rate, $\tan\delta$,
422 nano-indentation and increased hardness. To check the inter-connection between the
423 evolutions of these parameters during irradiation, a quantitative description was attempted.

424
425 Figure 6 shows the variations in the concentrations of amide groups (IR band at 1675 cm^{-1}),
426 gluconolactone (IR band at 1730 cm^{-1}), and ethers (IR band at 1150 cm^{-1}) during irradiation
427 (the film thickness was 25 microns, and the absorption coefficients were as follows: CONH:
428 $340\text{-}380\text{ L.mol}^{-1}.\text{cm}^{-1}$, gluconolactone: $650\text{-}700\text{ L.mol}^{-1}.\text{cm}^{-1}$, COC: $40\text{-}50\text{ L.mol}^{-1}.\text{cm}^{-1}$)
429 (from the literature) [Okamba-Diogo et al., 2014].



430
431 Figure 6: Concentration of the oxidation products (detected at 1675 cm^{-1} and at 1730
432 cm^{-1} in IR spectra) and disappearance of the C-O-C bond (detected at 1150 cm^{-1} in IR spectra)
433 versus irradiation time.

434 Figure 6 shows that the concentration of amide groups (1675 cm^{-1}) produced during
435 photooxidation was higher than the concentration of gluconolactone (1730 cm^{-1}). Indeed, the
436 concentration of gluconolactone generated after 600 hours of ageing corresponded to the
437 concentration of amide group after 100 hours of ageing.

438

439 To connect all the degradation criteria from the molecular scale to the macroscopic
 440 scale, we aimed to find kinetic information from the different parameters responsible for the
 441 degradation versus exposure time. We used a phenomenological model (Rose, Le Bras
 442 Bourbigot & Delobel, 1994) (Musto, Ragosta, Abbate & Scarinzi, 2008) to describe the
 443 kinetic processes of degradation as follows:

$$\frac{X(t)}{X(t=0)} = 1 - kt$$

$$X(t) = X(t=0). \exp(-kt)$$

444 where X(t) is the value of a selected parameter obtained for various times t, X (t=0) is
 445 the parameter value at t = 0 and k is the Arrhenius-type kinetic constant. The equation was
 446 applied to the experimental parameters X, such the absorbance A at 1730 cm⁻¹, nano-
 447 hardness, and T_g.

448 Table 2: Degradation rate (k) for the main degradation criteria of photooxidation

Parameters	Kinetic model	k (h ⁻¹ .10 ⁻³)	standard error (h ⁻¹ .10 ⁻³)	C.coeff χ ²
α C=O (1675 cm ⁻¹)	$\frac{A(t)}{A(t=0)} = 1 - kt$	0.475	0.05	0.999
Yellowing (A 400 nm)	$\frac{A(t)}{A(t=0)} = 1 - kt$	0.475	0.07	0.989
α C=O (1730 cm ⁻¹)	$A(t) = A(t=0). \exp(-kt)$	2.8	0.1	0.996
α COC	$A(t) = A(t=0). \exp(-kt)$	1.6	0.1	0.995
nano-Hardness/ Hardness	$A(t) = A(t=0). \exp(-kt)$	1.7	0.2	0.992
nano-Tg	$A(t)$	2.5	0.1	0.98
Roughness	$A(t)$	2.8	0.15	0.996

449

450

451 The results in Table 2 indicate that only the appearance of amide groups and the
452 increase in yellowing follow zero-order kinetics. The accumulation of gluconolactone and the
453 various parameters that were selected in an attempt to establish a correlation between the
454 variation in chemical structure and mechanical properties follow a first-order kinetic, and the
455 k values for the main parameters are similar (the average k value was $2 \cdot 10^{-3} \cdot \text{h}^{-1}$). The half-life
456 time was calculated from the kinetics, and the average $t_{1/2}$ value was approximately 200 hours.
457 The good agreement between the degradation-rate k-values of the different criteria confirms
458 the cross-correlation established. These results underline the difference in reactivity of all the
459 detected degradation species and confirm diverse routes of degradation.

460

461 **4. Conclusion**

462 Photooxidation of chitosan resulted in yellowing, crack formations, and an increase in
463 roughness. The increases in network density and nano-hardness are relevant in terms of a
464 reduction in the material's functional properties. A mechanism accounting for the main
465 degradation routes for chitosan photooxidation at the molecular scale was proposed. We
466 demonstrated the consequences of the chemical modifications on the material properties, and
467 we showed correlations between these chemical modifications and the evolution of the
468 mechanical properties. Our results allowed a « quantitative » correlation between the relevant
469 degradation criteria.

470

471

472 **Declaration of Interest**

473 None

474

475

476

Figure captions

477

478 Figure 1: IR spectra of chitosan films ($e = 25 \mu\text{m}$) before and after 24 h Soxhlet extraction in
479 MeOH (domain $1800\text{-}1000 \text{ cm}^{-1}$) and the chitosan powder in KBr pellets.

480

481 Figure 2: a) IR spectra of chitosan film ($e = 25 \mu\text{m}$) during photooxidation,
482 b) Subtracted IR spectra in carbonyl domain.

483

484 Figure 3: a) IR spectrum of a film ($e = 25 \mu\text{m}$) of chitosan blended with gluconolactone.
485 b) UV-visible spectra of a 600h photooxidized chitosan film before and after treatment with
486 2,4-DNPH.

487

488 Figure 4: UV-Visible spectra of chitosan film during photooxidation ($e = 25 \mu\text{m}$).

489

490 Figure 5: a) Change in roughness (\blacksquare) versus irradiation time (line is obtained by an
491 exponential fit).

492 b) Image of the chitosan film surface before and after 300 hours of irradiation.

493

494 Figure 6: Concentration of the oxidation products (detected at 1675 cm^{-1} and at 1730 cm^{-1} in
495 IR spectra) and loss of the C-O-C bond (detected at 1150 cm^{-1} in IR spectra) versus irradiation
496 time.

497

498 Table 1: Evolution of nano-hardness (nano-Hv) and nano- T_g as a function of irradiation time

499 Table 2: Degradation rate (k) for the main degradation criteria of photooxidation

500

501 Scheme 1: Chemical structure of chitosan

502 Scheme 2: Simplified photooxidation mechanism of chitosan

503

- 505 Abdelghany, A.M., Ayaad, D.M., Aboelkheir, A.M. (2019) The effects of prolonged UV
506 irradiation on the physicochemical characteristics of chitosan lamellar films modified with
507 nanoparticulate silver vanadate nanorods. *Polymer Bulletin*, doi :10.1007/s00289-019-03029-
508 x.
- 509 Aider, M. (2010) Chitosan application for active bio-based films production and potential in
510 the food industry: review, *LWT – Food science and Technology*, 43, 837-842.
- 511 Andrady, A.L., Torikai, A., Kobatake, T. (1996) Spectral Sensitivity of chitosan
512 photodegradation. *Journal of Applied Polymer Science*, 62, 1465-1471.
- 513 Berthumeyrie, S., Collin, S., Bussiere P.O., & Therias, S. (2014) Photooxidation of cellulose
514 nitrate: new insights into degradation mechanisms. *Journal of Hazardous Material*, 272, 137-
515 147.
- 516 Bussiere, P.-O., Rivaton, A., Therias, S., Gardette, J.-L. (2012) Multiscale Investigation of the
517 Poly(N-vinylcarbazole) Photoageing Mechanism. *The Journal of Physical Chemistry B*, 116,
518 802-812.
- 519 Collin, S., Bussiere, P.O., Therias, S., Lambert, J.M., Perdereau, J, Gardette J.L. (2012)
520 Physicochemical and mechanical impacts of photo-ageing on bisphenol a polycarbonate.
521 *Polymer Degradation and Stability*, 97, 2284-2293.
- 522 Fox, T. G., Flory, P. J. (1950) Second Order Transition Temperatures and Related Properties
523 of Polystyrene. I. Influence of Molecular Weight. *Journal of Applied Physics*, 21, 581-591.
- 524 Gamiz-Gonzalez, M.A., Correia, D.M., Lanceros-Mendes, S., Sencadas, V., Gomez Ribelles,
525 J.L., Vidaurre, A. (2017) Kinetic study of thermal degradation of chitosan as a function of
526 deacetylation degree. *Carbohydrate Polymers*, 167, 52-58.
- 527 Gaume, J., Wong-Wah-Chung, P., Rivaton, A., Therias, S., Gardette, J.L., (2011)
528 Photochemical behavior of PVA as an oxygen-barrier polymer for solar cell encapsulation.
529 *RSC Advances*, 1, 1471-1481.DOI: 10.1039/C1RA00350J.
- 530 Huang, Y., Wu, Y., Huang, W., Yang, F., Ren, X. (2013) Degradation of chitosan by
531 hydrodynamic cavitation. *Polymer Degradation and Stability*, 98(1), 37-43.

533 Kasaai, M.R. (2008) A review of several reported procedures to determine the degree of N-
534 acetylation for chitin and chitosan using infrared spectroscopy. *Carbohydrate Polymers*, 71,
535 497-508.

536 Kowalonek, J., (2017) Surface and thermal properties of UV-irradiated chitosan/poly(ethylene
537 oxide) blends. *Journal of Photochemistry and Photobiology, A : Chemistry*, 348, 209-218.

538 Lien, C.F., Molnar, E., Toman, P., Tsibouklis, J., Pilkington, G.J., Gorecki, D.C., E. Barbu, E.
539 (2012) In Vitro Assessment of Alkylglyceryl-Functionalized Chitosan nanoparticles as
540 permeating vectors for the blood – brain barrier, *Biomacromolecules*, 13, 1067-1073.

541 Moczek, L. & Nowakowska, M. (2007). Novel water-soluble photosensitizers from chitosan.
542 *Biomacromolecules*, 8, 433-438.

543 Moore, R.F. (1963) The photochemical degradation of polyamides and related model N-
544 alkylamides. *Polymer* 4: 493-513)

545 Mucha, M. & Pawlak, A. (2002) Complex study on chitosan degradability. *Polimery*, 47 (7-8),
546 509-516.

547 Musto, P., Ragosta, G., Abbate, M., Scarinzi, G. (2008) Photo-oxidation of high
548 performance epoxy networks: Correlation between the molecular mechanisms of degradation
549 and the viscoelastic and mechanical response. *Macromolecules*, 41, 5729-5743.

550 Nawi, M.A., Jawad, A.H., Sabar, S. ; Wan Ngah W.S. (2011) Photocatalytic-oxidation of
551 solid state chitosan by immobilized bilayer assembly of TiO₂-chitosan under a compact
552 household flurescent lamp irradiation. *Carbohydrate Polymers*, 83, 1146-1152.

553 Nazeer M.A., Yilgor, E., Yilgor, I. (2017) Intercalated chitosan/hydroxyapatite
554 nanocomposites : Promising materials for bone tissue engineering applications. *Carbohydrate*
555 *Polymers*, 17538-17546.

556 Ogawa, K., Yui, T., Okuyama, K. (2004). Three D structures of chitosan. *International*
557 *Journal of Biological Macromolecules*, 34, 1-8.

558 Okamba-Diogo, O., Richaud, E., Verdu, J., Fernagut, F., Guilment, J, Fayolle, B., (2014).
559 Molecular and macromolecular structure changes in polyamide 11 during thermal oxidation,
560 *Polymer Degradation and Stability*, 108, 123-132.

561 Oliver, W.C., Pharr, G.M. (1992) An improved technique for determining hardness and
562 elastic modulus using load and displacement sensing indentation experiments. *Journal of*
563 *Materials Research*, 7, 1564-1583.

564 Philippart, J.L., Sinturel, C., Gardette, J.L. (1997). Influence of light intensity on the
565 photooxidation of polypropylene. *Polymer Degradation and Stability*, 58 (3), 261-268.

566 Rideal, E.K. & J. S. Mitchell, J.S. (1937) Photochemical reactions in monolayers I-
567 Photochemical properties of the ketoimino linkage. *Proc. Roy. Soc. (London)*, 159, 206.

568 Rinaudo, M., Pavlov, G., J. Desbrieres, J. (1999) Influence of acetic acid concentration on the
569 solubilization of chitosan. *Polymer*, 40, 7029-7032.

570 Rose, N., Le Bras, M., Bourbigot, S., Delobel, R. (1994) Thermal oxidative degradation of
571 epoxy resins: evaluation of their heat resistance using invariant kinetic parameters. *Polymer*
572 *Degradation and Stability*, 45, 387-397.

573 Scott, G. (1995) Initiation processes in polymer degradation. *Polymer Degradation and*
574 *Stability*, 48 (3), 315-324.

575 Sharkey, W.H. & Mochel, W.E. (1959) Mechanism of the Photooxidation of Amides. *J. Am.*
576 *Chem. Soc.* (8-12), 3000-3005.

577 Sionkowska, A., Wisniewski, M., Skopinska, J., Vicini, S., Marsano, E. (2005) The influence
578 of UV irradiation on the mechanical properties of chitosan/poly(vinyl pyrrolidone) blends.
579 *Polymer Degradation and Stability*, 88 (2), 261-267.

580 Sionkowska, A., Kazmarek, H., Wisniewski, M., Skopinska, J., Lazare, S., Tokarev, V.
581 (2006). The influence of UV irradiation on the surface of chitosan films. *Surface Science*,
582 600, 3775-3779.

583 Sionkowska, A., Skopinska-Wisniewska, J., Planecka, A., Kozłowska, J. (2010) The
584 influence of UV irradiation on the properties of chitosan films containing keratin. *Polymer*
585 *Degradation and Stability*, 95(12), 2486-2491.

586 Sionkowska, A., Planecka, A., Kozłowska, J., Skopinska-Wisniewska, J., Los, P. (2011)
587 Weathering of chitosan films in the presence of low- and high- molecular weight additives,
588 *Carbohydrate Polymers*, 84, 900-906.

589 Sionkowska, A., Planecka, A., Lewandowska, K., Kaczmarek, B., Szarszewska, P. (2013).
590 Influence of UV-irradiation on molecular weight of chitosan, *Progress on Chemistry and*
591 *Application of Chitin and Its derivatives*, 18, 21-28.

592 Sionkowska, A., Planecka, A., Lewandowska, K., Michalska, M. (2014) The influence of
593 UV-irradiation on thermal and mechanical properties of chitosan and silk fibroin mixtures.
594 *Journal of Photochemistry and Photobiology, B : Biology*, 140, 301-305.

595 Sionkowska, A., Kaczmarek, B., Gnatowska, M., Kowalonek, J. (2015) The influence of UV-
596 irradiation on chitosan modified by the tannic acid addition. *Journal of Photochemistry and*
597 *Photobiology, B : Biology*, 148, 333-339.

598 Synytsya, A., Grafova, M., Slepicka, P., Gedeon, O., Synytsya, A. (2012). Modification of
599 Chitosan-Methylcellulose composite films with meso-Tetrakis(4-sulfonatophenyl)porphyrin.
600 *Biomacromolecules*, 13(2), 489-498.

601 Taskn, P., Cansag, H., Sen, M. (2014) The effect of degree of deacetylation on the radiation
602 induced degradation of chitosan. *Radiation Physics and Chemistry*, 94, 236-239.

603 Tchemtchoua, V.T., Atanasova, G., Aqil, A., Filee, P., Garbacki, N., Vanhootehem, O.,
604 Deroanne, C., Noël, A., Jerome, C., B. Nusgens, B. (2011) Development of a chitosan
605 nanofibrillar scaffold for skin repair and regeneration, *Biomacromolecules*, 12(9), 3194-3204.

606 Valentin, R., Bonelli, B., Garrone, E., Di Renzo, F., Quignard, F. (2007) Accessibility of the
607 Functional Groups of Chitosan aerogel probed by FT-IR monitored deuteration.
608 *Biomacromolecules*, 8, 3646-3650.

609 Villar-Chavero, M.M., Dominguez, J.C., Alonso, M.V., Oliet, M., Rodriguez, F. (2018)
610 Thermal and kinetics of the degradation of chitosan with different deacetylation degrees under
611 oxidizing atmosphere. *Thermochimica Acta*, 670, 18-26.

612 Wang, S-M., Huang, Q-Z., Wang, Q-S. (2005) Study on the synergetic degradation of
613 chitosan with ultraviolet light and hydrogen peroxide. *Carbohydrate research* 340(6), 1143-
614 1147.

615 Wasikiewicz, J.M., Yoshii, F., Nagasawa, N., Wach, R.A., Mitomo, H. (2005) Degradation of
616 chitosan and sodium alginate by gamma radiation, sonochemical and ultraviolet methods.
617 *Radiation Physics and Chemistry*, 73(5), 287-295. DOI: 10.1016/j.radphyschem.2004.09.021

618 Wasikiewicz, J.M., Yeates, S.G., (2013) « Green » molecular weight degradation of chitosan
619 using microwave irradiation. *Polymer Degradation and Stability*, 98(4), 863-867.

620 Wilhelm, C. & Gardette, J.L. (1994) Infrared identification of carboxylic acids formed in
621 polymer photooxidation. *Journal of Applied Polymer Science*, 51(8), 1411-1420.

- 622 Zawadzki, J. & Kaczmarek, H. (2010) Thermal treatment of chitosan in various conditions.
623 *Carbohydrate Polymers*, 80, 394-400.